

Solar Wind Turbulence Around Mars: Relation Between The Energy Cascade Rate And The Proton Cyclotron Waves Activity

NAHUEL ANDRÉS ^{1,2} NORBERTO ROMANELLI ^{3,4} LINA Z. HADID ^{5,6} FOUAD SAHRAOUI,⁵
GINA DI BRACCIO ³ AND JASPER HALEKAS ⁷

¹*Instituto de Astronomía y Física del Espacio, CONICET-UBA, Ciudad Universitaria, 1428, Buenos Aires, Argentina*

²*Departamento de Física, UBA, Ciudad Universitaria, 1428, Buenos Aires, Argentina*

³*Solar System Exploration Division, NASA Goddard Space Flight Center, Greenbelt, MD, USA*

⁴*CRESST II, University of Maryland, Baltimore County, Baltimore, MD, USA.*

⁵*LPP, CNRS, École polytechnique, Institut Polytechnique de Paris, Sorbonne Université, F-91128 Palaiseau, France*

⁶*European Space Agency, ESTEC, Noordwijk, Netherlands*

⁷*Department of Physics and Astronomy, University of Iowa, Iowa City, Iowa, USA*

Submitted to ApJ

ABSTRACT

The first estimation of the incompressible energy cascade rate at magnetohydrodynamic (MHD) scales in the plasma upstream of the Martian bow shock is obtained, making use of magnetic field and plasma observations provided by Mars Atmosphere and Volatile Evolution (MAVEN) over 600 orbits. In particular, the energy cascade rate is computed for events with and without proton cyclotron wave (PCW) activity, for time intervals when MAVEN was in the solar wind with no magnetic connection to the bow shock. It is shown that the nonlinear cascade of energy at the MHD scales is slightly amplified when PCWs are present in the plasma, around the Martian perihelion. In addition, the analysis of the normalized cross helicity and residual energy for the turbulent fluctuations shows the presence of Alfvénic and non-Alfvénic fluctuations in a magnetic dominant regime for the majority of the cases.

1. INTRODUCTION

Turbulence is a unique phenomenon present in several space environments, like the solar corona (Hendrix & Van Hoven 1996; Dmitruk et al. 2002), planetary environments (Sahraoui et al. 2020) or the solar wind (Bruno & Carbone 2005; Matthaeus & Velli 2011). In particular, solar wind turbulence is partially characterized by an inertial range, where energy is transferred without dissipation through different spatial and temporal scales (e.g., Frisch 1995). Typically, in the largest magnetohydrodynamic (MHD) scales, the solar wind magnetic spectrum presents a $-5/3$ slope (Kolmogorov 1941a,b; Matthaeus & Goldstein 1982; Leamon et al. 1998; Chen 2016), which is generally compatible with a constant energy cascade rate as a function of such scales (Sorriso-Valvo et al. 2007; Marino et al. 2008; Coburn et al. 2014; Coburn et al. 2015; Hadid et al. 2017). A constant energy cascade

rate reflects a well accepted idea that large (MHD) scale turbulence serves as a reservoir of energy that cascades down to the smallest scales, where it can be dissipated by kinetic effects (e.g., [Leamon et al. 1998](#); [Sahraoui et al. 2009](#); [Alexandrova et al. 2009](#); [Andrés et al. 2014](#)).

Assuming spatial homogeneity and full isotropy, an exact relation for fully developed incompressible MHD turbulence can be derived ([Politano & Pouquet 1998a,b](#)). Among its potential applications (e.g., [Weygand et al. 2007](#); [Matthaeus et al. 1999](#); [MacBride et al. 2008](#); [Benzi et al. 1993](#); [Grossmann et al. 1997](#); [Andrés & Banerjee 2019](#)), the exact relation provides a precise computation of the amount of energy per unit time and volume (or heating rate) as a function of the velocity and magnetic correlation functions. The MHD exact relation and its connection with the nonlinear energy cascade rate has been numerically validated for both incompressible and compressible MHD turbulence ([Andrés et al. 2018](#)), and has been generalized to include sub-ion scale effects ([Andrés et al. 2018, 2019](#); [Hadid et al. 2018](#); [Hellinger et al. 2018](#); [Ferrand et al. 2019](#); [Banerjee & Andrés 2020](#)). Estimations of the energy cascade rate in the inertial range of solar wind turbulence have been previously computed at 1 Astronomical Unit (AU) (see, [Marino et al. 2008](#); [Coburn et al. 2014](#); [Coburn et al. 2015](#); [Banerjee et al. 2016](#); [Hadid et al. 2017](#)) and more recently at ~ 0.2 AU ([Bandyopadhyay et al. 2020](#); [Chen et al. 2020](#)). In particular, [Hadid et al. \(2017\)](#) have investigated in detail the role of the compressible fluctuations ([Banerjee & Galtier 2013](#); [Andrés & Sahraoui 2017](#)) in modifying the energy cascade rate with respect to the prediction of the incompressible MHD model, based in situ data from the THEMIS/ARTEMIS spacecraft in the fast and slow solar wind.

The induced magnetosphere of Mars is formed as a result of the interaction between the solar wind and the planet's atmosphere, including its exosphere, ionosphere and the crustal magnetic fields ([Acuña 1998, 1999](#)). This interaction starts upstream of the Martian bow shock, due to the lack of an intrinsic global planetary magnetic field and the presence of an extended hydrogen exosphere (e.g., [Chaffin et al. 2015](#)). The response of this atmospheric obstacle is significantly modified by time-dependent physical processes (e.g., [Edberg et al. 2010](#); [Jakosky et al. 2015b](#); [Romanelli et al. 2018a](#)), as a result of temporal variability of the planetary and solar wind properties over different timescales (e.g., [Edberg et al. 2009](#); [Modolo et al. 2012](#); [Ma et al. 2014](#); [Fang et al. 2015](#); [Romanelli et al. 2018b, 2019](#)).

The seasonal variability of the Martian hydrogen exosphere has been identified by several spacecraft ([Bhattacharyya et al. 2015](#); [Chaffin et al. 2014](#); [Clarke et al. 2014, 2017](#); [Halekas et al. 2017](#)). In particular, such variability exhibits higher column densities mostly observed around the Martian perihelion and lower column densities around aphelion ([Halekas 2017](#)). The Martian exosphere is subject to several ionizing mechanisms giving rise to newborn planetary protons, allowing one to indirectly observe such seasonal dependence with plasma instruments (e.g., [Yamauchi et al. 2015](#); [Rahmati et al. 2017](#)). For instance, [Yamauchi et al. \(2015\)](#) reported a strong correlation between the detection rate of pickup ions originating from ionized exospheric hydrogen and the Martian heliocentric distance, based on Mars Express Ion Mass Analyzer observations. Higher pickup ions detection rates were observed when Mars is near perihelion. Moreover, when available, the measurement of the resulting proton velocity distribution function at these altitudes is composed of a core of solar wind particles and a non thermal proton population due to the presence of newborn planetary ions (seen in the solar wind reference frame). Such particle velocity distribution function is highly unstable and can give rise to several ultra-low frequency plasma waves ([Wu & Davidson 1972](#); [Wu & Hartle 1974](#); [Brinca 1991](#); [Gary 1991](#); [Mazelle & Neubauer 1993](#); [Cowee et al. 2012](#)).

Despite their capability to excite different plasma waves, the relative velocity between the newborn planetary proton reference frame (very close to the planetary and spacecraft rest frames) and the solar wind is also responsible for a Doppler shift that defines the observed wave frequency near the local proton cyclotron frequency in the spacecraft reference frame (e.g., [Russell et al. 1990](#); [Brain 2002](#); [Mazelle et al. 2004](#); [Romanelli et al. 2013, 2016](#); [Ruhunusiri et al. 2015, 2016](#); [Liu et al. 2020](#)). These waves are therefore called proton cyclotron waves (PCWs). Variability in the PCWs occurrence rate has been observed based on Mars Global Surveyor magnetic field data ([Romanelli et al. 2013](#); [Bertucci et al. 2013](#)) and more recently with MAVEN Magnetometer (MAG) observations ([Romanelli et al. 2016](#); [Jakosky et al. 2015a](#); [Connerney et al. 2015](#)). In particular, [Romanelli et al. \(2016\)](#) have analyzed MAG observations between October 2014 and March 2016. The authors reported that the PCWs occurrence rate upstream of the Martian bow shock varies with time and takes higher values near the Martian perihelion. Such long term trend was associated with higher hydrogen exospheric densities around that orbital position (derived from numerical simulations) and was also in agreement with the long term trend observed in the irradiances in the 121-122 nm range by MAVEN extreme ultra-violet monitor (EUVM) measurements ([Eparvier et al. 2015](#)), which provide a proxy to study the temporal variability of the photoionization frequency of the neutral H exosphere.

[Ruhunusiri et al. \(2017\)](#) have characterized magnetic energy spectra in the Mars plasma environment using the MAVEN MAG observations, in the frequency range 0.005 Hz to 16 Hz. By computing the spectral indices for the magnetic energy, the authors showed a wide range of values in the upstream solar wind and the magnetosheath plasma. Also, they observed a seasonal variability of the spectral indices, indicative of a clear connection with the seasonal variability of the PCWs. Nevertheless, to the best of our knowledge, no estimation of the energy cascade rate has been reported yet in the Martian plasma environment. In the present Letter, we aim to extend the current state of knowledge of the solar wind turbulence upstream the Martian shock by computing for the first time the energy transfer rate using an exact relation for fully development turbulence. Using both magnetic field and plasma moments observations at $\sim 1.38 - 1.67$ AU, we investigate how turbulence is affected not only by the heliocentric distance, but also by the presence of PCWs. The study is structured as follows: in Section 2, we present the theoretical incompressible MHD model and a brief description of the exact relation. In Section 3.1 and 3.2 we briefly describe the capabilities of the MAVEN instruments and the conditions that each turbulent event must fulfil, respectively. In Sections 3.3, 3.4 and 3.5 we present the main results of our analysis. Finally, the discussion and conclusions are developed in Section 4.

2. INCOMPRESSIBLE MHD TURBULENCE

The three-dimensional (3D) incompressible MHD equations are the momentum equation for the velocity field \mathbf{u} (in which the Lorentz force is included), the induction equation for the magnetic field \mathbf{B} , and the solenoid condition for both fields. These equations can be written as,

$$\frac{\partial \mathbf{u}}{\partial t} = -\mathbf{u} \cdot \nabla \mathbf{u} + \mathbf{u}_A \cdot \nabla \mathbf{u}_A - \frac{1}{\rho_0} \nabla (P + P_M) + \mathbf{f}_k + \mathbf{d}_k, \quad (1)$$

$$\frac{\partial \mathbf{u}_A}{\partial t} = -\mathbf{u} \cdot \nabla \mathbf{u}_A + \mathbf{u}_A \cdot \nabla \mathbf{u} + \mathbf{f}_m + \mathbf{d}_m, \quad (2)$$

$$\nabla \cdot \mathbf{u} = 0, \quad (3)$$

$$\nabla \cdot \mathbf{u}_A = 0 \quad (4)$$

where we have defined the incompressible Alfvén velocity $\mathbf{u}_A \equiv \mathbf{B}/\sqrt{4\pi\rho_0}$ (where ρ_0 the mean mass density) and $P_M \equiv \rho_0 u_A^2/2$ is the magnetic pressure. Then, both field variables, \mathbf{u} and \mathbf{u}_A , are expressed in speed units. Finally, $\mathbf{f}_{k,m}$ are respectively a mechanical and the curl of the electromotive large-scale forcings, and $\mathbf{d}_{k,m}$ are respectively the small-scale kinetic and magnetic dissipation terms (Andrés et al. 2016b; Banerjee & Kritsuk 2018).

Using Eq. (1)-(4) and following the usual assumptions for fully developed homogeneous turbulence (i.e., infinite kinetic and magnetic Reynolds numbers and a steady state with a balance between forcing and dissipation (see, e.g. Andrés & Sahraroui 2017), an exact relation for incompressible MHD turbulence can be obtained as (Politano & Pouquet 1998a,b),

$$-4\varepsilon = \rho_0 \nabla_\ell \cdot \langle (\delta\mathbf{u} \cdot \delta\mathbf{u} + \delta\mathbf{u}_A \cdot \delta\mathbf{u}_A)\delta\mathbf{u} - (\delta\mathbf{u} \cdot \delta\mathbf{u}_A + \delta\mathbf{u}_A \cdot \delta\mathbf{u})\delta\mathbf{u}_A \rangle, \quad (5)$$

where ε is the total energy cascade rate per unit volume. Fields are evaluated at position \mathbf{x} or $\mathbf{x}' = \mathbf{x} + \boldsymbol{\ell}$; in the latter case a prime is added to the field. The angular bracket $\langle \cdot \rangle$ denotes an ensemble average (Batchelor 1953), which is taken here as time average assuming ergodicity. Finally, we have introduced the usual increments definition, i.e., $\delta\alpha \equiv \alpha' - \alpha$. Here we are interested in estimating ε from Eq. (7), which is fully defined by velocity and magnetic field increments (or fluctuations) that we can estimate from MAVEN observations.

3. ANALYSIS AND RESULTS

3.1. MAVEN observations

The MAVEN spacecraft was launched in November 2013 and arrived at Mars in September 2014. The orbit had a nominal periapsis altitude of 150 km, an apoapsis altitude of 6220 km, and an orbital period of about 4.5 hours (Jakosky et al. 2015a). The selected apoapsis altitude, orbital period and inclination (75°) allow orbital precession in both local time and latitude of the spacecraft periapsis. In addition, the extent of the MAVEN apoapsis allows sampling of solar wind properties upstream of its bow shock. The MAVEN Magnetometer (MAG) provides vector magnetic field measurements with a 32 Hz maximum sampling frequency and absolute vector accuracy of 0.05% (Connerney et al. 2015). MAVEN's Solar Wind Ion Analyzer (SWIA) is an energy and angular ion spectrometer covering an energy range between 25 eV/q and 25 keV/q with a field of view of 360°×90° (Halekas et al. 2015). In this study, we have analyzed MAVEN MAG and SWIA data sets as follows. Magnetic field observations with 32 Hz cadence are analyzed to discriminate events in the pristine solar wind with PCWs and without wave activity. To estimate the energy cascade rate at MHD scales (i.e., frequencies below ~ 0.1 Hz) we averaged the magnetic field data over 4 s to match SWIA onboard moments cadence (Halekas et al. 2015). In particular, in this study we have used SWIA solar wind density and velocity onboard computed moments. Such moments assume a plasma made of protons, a very good approximation upstream from the Martian bow shock (Halekas et al. 2017).

As discussed in the Introduction, Romanelli et al. (2016) have found that the PCWs occurrence rate increases (up to $\sim 50\%$) when Mars is close to the perihelion (1.38 AU) on December 12 2014 and remains relatively low and constant ($\sim 25\%$) after reaching the Martian Northern Spring Equinox-Southern Autumn Equinox (NSE-SAE). Also, the authors concluded that the increment in the PCWs occurrence rate cannot be the result of biases associated with MAVEN's spatial coverage of the upstream region or of the differences in the spatial distribution of the crustal magnetic fields. Therefore, to investigate how PCWs activity may affect the nonlinear transfer of energy, we consider

two data sets. Set A contains observations from December 1 2014 until January 31 2015; and set B from January 1, 2016 until February 29, 2016. Set A includes MAVEN observations around perihelion and a local maximum of PCWs activity, while set B includes the Martian Northern Summer Solstice-Southern Winter Solstice (NSS-SWS) that took place on January 3 2016 (and corresponds to a local minimum of waves activity).

3.2. Selection criteria

For sets A and B (~ 330 orbits per set), during time periods when MAVEN was traveling in the solar wind with no connection to the shock (Gruesbeck et al. 2018), we looked for intervals in which the number density fluctuation level was lower than 20% (to be as close as possible to the incompressibility condition). Moreover, in order to have a reliable estimate of the energy cascade rate ε (both its sign and its absolute value (Halekas et al. 2017)) we only consider the events in which the θ_{uB} (the angle between the magnetic and velocity field) was relatively stationary (Andrés et al. 2019). The time interval of each MAVEN orbit that fulfill these conditions were divided into a series of sample events with a duration of 30 minutes. This duration ensures having at least one correlation time of the turbulent fluctuations (Hadid et al. 2017; Marquette et al. 2018). Finally, for set A (set B) we considered only cases when PCWs activity was present (absent). By doing this, we can assess the effects that the PCWs may have on the solar wind turbulence. This selection resulted in 184 and 208 events for sets A and B, respectively.

Figure 1 shows two examples of the typical events analyzed in the present Letter (panels (a)-(h) show an example from set A, and panels (i)-(p) from set B). Figure 1 (a)-(f) show the time series for the proton and Alfvén velocity field components in Mars-centered Solar Orbital (MSO) coordinate system (where the \mathbf{x} -axis points from Mars to the Sun, \mathbf{z} -axis is perpendicular to Mars' orbital plane and is positive toward the ecliptic north; the \mathbf{y} -axis completes the right-handed system). Figure 1 (g)-(h) show the angle between the magnetic and velocity field θ_{uB} and the density fluctuation level (i.e., $\Delta n/\langle n \rangle$), respectively. As can be seen, although both examples show approximately the same level of density fluctuations and the same θ_{uB} angle, there is a sharp contrast with and without clear wave activity present in the left and right panel, respectively.

Figure 2 shows the probability distribution functions (PDFs) for all the analyzed events in both sets for (a)-(c) the number density, velocity, and Alfvén velocity field absolute values and for (d)-(f) its fluctuation amplitudes, respectively. Both sets have similar distributions for the fluctuation values.

3.3. PSD of the magnetic field fluctuations

To determine if a given time interval presents PCWs activity or not, we used a criterion similar to the one in Romanelli et al. (2016). An event is considered to present PCWs activity when the magnetic energy power spectral density (PSD) displays an increase in a frequency interval centered around the local proton cyclotron frequency f_{ci} when compared to two contiguous windows of width $0.2 f_{ci}$. More precisely,

$$\max\{\text{PSD}[B(f)]|_{0.8f_{ci}}^{1.2f_{ci}}\} > \max\{\text{PSD}[B(f)]|_{1.2f_{ci}}^{1.4f_{ci}}\}, \max\{\text{PSD}[B(f)]|_{0.6f_{ci}}^{0.8f_{ci}}\} \quad (6)$$

where \max corresponds to the maximum value in the PSD in the corresponding window.

Figure 3 (a) and (b) show the PSD for all the events in sets A and B, respectively. For reference, we plot a straight line with Kolmogorov-like slope (i.e., $-5/3$) in both cases. As we expected, all events

near the Martian perihelion (i.e., set A) show a clear peak in their PSD near the proton cyclotron frequency f_{ci} . Moreover, all the cases analyzed in the present Letter show a Kolmogorov-like slope in the MHD scales (see, [Ruhunusiri et al. 2017](#)). Figure 4 (a) and (b) show the MAVEN location (where $R_{\text{MSO}} = \sqrt{y_{\text{MSO}}^2 + z_{\text{MSO}}^2}$) for each event for sets A and B, respectively. The gray dashed line corresponds to the best fit of the bow shock reported by [Gruesbeck et al. \(2018\)](#). In that study, the authors presented a model of the Martian bow shock as a three dimensional surface making use of 1000 crossings observed by MAVEN. As shown in Figure 4 insets, sets A and B present some differences in the cylindrical MSO spatial distributions. In particular, the statistical distribution of observations corresponding to set B are slightly closer to the Martian bow shock fit.

3.4. Energy cascade rates

To compute the right hand side of Eq. (5), we constructed temporal correlation functions of the different turbulent fields at different time lags τ in the interval [4,1800] s, which allows covering the MHD inertial range ([Ruhunusiri et al. 2017](#); [Hadid et al. 2017](#)). More precisely, assuming isotropic turbulence and the Taylor hypothesis (i.e., $\ell \equiv \tau V$, where V is the mean plasma flow speed and $\ell = |\ell|$ is the longitudinal distance), Eq. (5) can be expressed as a function of time lags τ . Since we are dealing with single spacecraft measurements, we assume that the isotropic energy cascade rate is representative of the real cascade rate. In particular, while Eq. (5) includes increments in all the spatial directions, here we only include the increments in the longitudinal direction ℓ . Therefore, for each event in both sets, the energy cascade rate is computed as,

$$\varepsilon = \rho_0 \langle [(\delta \mathbf{u} \cdot \delta \mathbf{u} + \delta \mathbf{u}_A \cdot \delta \mathbf{u}_A) \delta u_\ell - (\delta \mathbf{u} \cdot \delta \mathbf{u}_A + \delta \mathbf{u}_A \cdot \delta \mathbf{u}) \delta u_{A\ell}] / (-4/3\ell) \rangle. \quad (7)$$

Figure 5 (a) and (b) show the absolute value of the energy cascade rate as a function of the time lag (τ) for both sets. Figure 5 (c) shows the histogram for the (log) mean values $\log \langle |\varepsilon| \rangle_{\text{MHD}}$ in the MHD scales ($\tau = 5 \times 10^2 - 1.5 \times 10^3$ s). It is worth emphasizing that if ε is changing significantly in amplitude and/or sign, then the resulting mean values would not be reliable (see, e.g., [Hadid et al. 2018](#); [Andrés et al. 2019](#)). Therefore, as we mentioned before, we kept only the intervals for which the cascade rate shows a constant (negative or positive) sign for all the time lags in the MHD range. By doing so, the mean value of ε for each event is robust and so is its absolute value ([Coburn et al. 2015](#); [Hadid et al. 2018](#)). The only limitation of analyzing the non-signed ε is related to the direct vs. inverse nature of the energy cascade rate. This is because the convergence of the sign of ε is more stringent than its absolute value (see, [Coburn et al. 2015](#); [Hadid et al. 2018](#)), thus demanding a much larger statistical sample than the one considered in the present work. For both data sets A and B, the cascade rate values are lower than the averaged value observed at 1 AU, $\varepsilon \sim 10^{-16} - 10^{-17}$ J m⁻³ s⁻¹ ([Hadid et al. 2018](#)). Also, it is worth mentioning that the energy cascade rate increases slightly when PCWs are present in the solar wind, based on our statistical analysis.

3.5. Alfvénic fluctuations

The cross helicity $H_c = \langle \mathbf{u} \cdot \mathbf{u}_A \rangle$ and the total energy $E_T \equiv (\langle |\mathbf{u}|^2 \rangle + \langle |\mathbf{u}_A|^2 \rangle) / 2$ (where \mathbf{u} and \mathbf{u}_A are the proton and Alfvén velocities fluctuations) are the two rugged invariant of the ideal incompressible MHD model (see Eqs. 1-4). The dimensionless measure of the normalized cross-helicity corresponds to $\sigma_c \equiv H_c / E_T$, with $-1 \leq \sigma_c \leq 1$. Usually, fluctuations with $|\sigma_c| \sim 1$ are described as being

Alfvénic. Another related measurement to quantify the relative energy present in the kinetic and magnetic fluctuations is the normalized residual energy $\sigma_r \equiv (\langle |\mathbf{u}|^2 \rangle - \langle |\mathbf{u}_A|^2 \rangle) / E_T$. This parameter also ranges between -1 and 1.

Figure 6 shows the scatter plot of σ_r as a function of σ_c , for both sets A and B, respectively. The colorbar corresponds to the mean value of the energy cascade rate in the MHD scales $\langle |\varepsilon| \rangle_{\text{MHD}}$. The statistical results show a wide variety of possible values of σ_r and σ_c , independently of the presence of PCWs. However, for set B, the events gather around $|\sigma_c| \sim 0.75$ and $\sigma_r \sim -0.4$.

4. DISCUSSIONS AND CONCLUSIONS

In the present work, we analyzed two data sets by considering separately the cases with (set A) and without PCWs (set B). In agreement with previous studies, our findings are consistent with the seasonal variability of PCWs (Romanelli et al. 2013; Bertucci et al. 2013; Romanelli et al. 2016). As shown in Figure 4, the spatial distributions of the cylindrical MSO coordinates associated with the events in sets A and B display some differences. However, as reported in Romanelli et al. (2016), the PCWs occurrence rate temporal variability upstream from the bow shock cannot be associated with biases in the spatial coverage of MAVEN or with changes in the background magnetic fields. Moreover, in this work we restricted our analysis to time intervals with no connection to the Martian bow shock to avoid effects associated with backstreaming particles (Mazelle et al. 2018). Our statistical results show slopes compatible with a Kolmogorov scaling in the largest MHD scales in both sets. Ruhunusiri et al. (2017) determined spectra of magnetic field fluctuations in order to characterize turbulence in the Mars plasma environment. Using 512 s sliding windows, the authors found that magnetic spectrum slopes present different values. In particular, they found that the slope is typically ~ -1.2 at the solar wind (in the MHD scales), which differs from the Kolmogorov spectrum. This discrepancy between the computed slopes could be due to several factors: i) we are including only the cases where the cascade rate and the angle θ_{uB} are approximately constant; ii) the sliding window size used in Ruhunusiri et al. (2017) may not include enough correlation times to yield reliable PSD slopes; and iii) we are separating between PCWs and no waves events, while Ruhunusiri et al. (2017) included all the available data. It is worth mentioning that Gurnett et al. (2010) showed that the magnetic field fluctuations have a Kolmogorov scaling using magnetic field values derived from electron cyclotron echoes from Mars Express observations. Also, the $f^{-5/3}$ spectrum for the magnetic energy is theoretically compatible with our constant energy cascade rate assumption (Andrés et al. 2016b,a).

We found that the energy cascade rate at Mars ($\sim 1.38 - 1.67$ AU) decreases compared with previous results at 1 AU and smaller distances from the Sun (see, Matthaeus & Velli 2011; Bruno & Carbone 2005; Hadid et al. 2017; Bandyopadhyay et al. 2020). In particular, the statistical results for the data set B (no presence of PCWs activity) show a decrease of $|\varepsilon|$ of at least 1 order of magnitude with respect to the value at 1 AU (i.e., $10^{-16} - 10^{-17}$ J m⁻³ s⁻¹) (Hadid et al. 2018). Recent observations have shown that the energy cascade rate becomes larger closer to the Sun (Bandyopadhyay et al. 2020). Probably, these large values of the energy cascade rate are due to strong forcing process occurring closer to the Sun's corona. However, a precise study comparing the energy cascade rate at other different heliocentric distances can be found elsewhere (e.g., Bruno & Carbone 2005).

In addition, we observe a slight increase in the transfer of energy when waves activity is present in the plasma (set A). These results suggest that PCWs at the sub ion scales may affect the turbulence properties at the MHD scales. In other words, while Eq. (7) is valid *only* in the MHD inertial range,

our results suggest that the instabilities and consequent nonlinear waves at frequencies $\sim f_{ci}$ may affect the largest MHD scales (Osman et al. 2013; Hadid et al. 2018). It is worth mentioning that, although several theoretical papers have shown that newborn planetary ions are capable of providing the free energy for the presence of PCWs (e.g., Brinca 1991), the PCWs observed upstream from the Martian bow shock are nonlinear and likely not saturated (Cowee et al. 2012). Thus, while the observed increase in $|\varepsilon|$ in correlation with PCWs activity has not been reported before, an analysis of the local velocity distribution functions is still needed to better characterize the growing stage of the observed PCWs and its connection with these results (e.g., Mazelle et al. 2000, 2003; Romanelli et al. 2018). Moreover, a comparative analysis of these energy cascade rate estimates with the ones upstream from the bow shocks of Venus and active comets would allow us to better determine the significance of such correlation. Indeed, waves with frequencies close to the local proton and water group ion cyclotron frequency have been reported upstream from Venus and several active comets, respectively, and therefore might also affect the pristine solar wind energy cascade rates (see, Mazelle et al. 1997; Delva et al. 2015).

While both sets show similar values in the parameter space of number density, velocity and Alfvén velocity fields values, our results show a wide variability in the possible values of σ_c and σ_r . In particular, the events in set B correspond to Alfvénic and magnetic dominant fluctuations ($|\sigma_c| \sim 0.75$ and $\sigma_r \sim -0.4$). Interestingly, these events correspond to the higher values of the cascade rate in the set B. Moreover, for both sets the events have mainly negative σ_r values with a majority gathering around $\sigma_r \sim -0.25$ and $\sigma_r \sim -0.4$, respectively. This majority of events in the magnetic dominant regime is compatible with previous results between 1 and 8 AU (Roberts et al. 1990; Bruno et al. 2007; Matthaeus et al. 2008; Halekas et al. 2017). In particular, Halekas et al. (2017) have investigated the spatial distributions of σ_r and σ_c using 30 minutes time intervals with a 45 s cadence. Separating observations into four subsets based on the B_y sign and the time range (near perihelion or aphelion), the authors found that the temporal decrease in σ_c appears to be equally present in all upstream regions sampled by MAVEN. Our results using 4 s or 45 s (not shown here) cadence exhibit a similar statistical trend. Therefore, the PCWs activity is not affecting significantly the mean value of the statistical distributions of σ_r and σ_c . Slight differences with Halekas et al. (2017) are probably due to the considered selection criteria.

Finally, in this study we have not computed the compressible component of the energy cascade rate (Banerjee & Galtier 2013; Andrés & Sahraoui 2017). In particular, we expect to obtain a strong increase in the nonlinear cascade rate of energy in the Martian magnetosheath, where compressibility plays a major role, like in the Earth’s magnetosheath (Hadid et al. 2018; Andrés et al. 2019). In addition, we emphasize that we can not definitively state that the presence of PCWs is the ultimate responsible for the energy cascade rate increase. Indeed, another possible reason that could explain the observed increase in the cascade rate amplitude might be the heliocentric distance variation along Mars orbit. The presence of waves, as the energy cascade rate amplitude, are both dependent on the Martian heliocentric distance. Therefore, to decouple effects due to the presence of PCWs, the cascade rate amplitude and the heliocentric distance is necessary to consider additional magnetic field and plasma data sets. Furthermore, a possible seasonal variability of the incompressible and/or compressible energy cascade rate may be present in the Martian environment as well. These studies will be part of an ongoing work.

ACKNOWLEDGMENTS

N.A., L.H.Z. and F.S. acknowledge financial support from CNRS/CONICET Laboratoire International Associé (LIA) MAGNETO. We thank the entire MAVEN team and instrument leads for data access and support. N.A. acknowledge financial support from the Agencia de Promoción Científica y Tecnológica (Argentina) through grants PICT 2018 1095. MAVEN data are publicly available through the Planetary Data System (<https://pds-ppi.igpp.ucla.edu/index.jsp>).

REFERENCES

- Acuña, M. H. 1998, *Science*, 279, 1676
 —. 1999, *Science*, 284, 790
 Alexandrova, O., Saur, J., Lacombe, C., et al. 2009, *Phys. Rev. Lett.*, 103, 165003, doi: [10.1103/PhysRevLett.103.165003](https://doi.org/10.1103/PhysRevLett.103.165003)
 Andrés, N., & Banerjee, S. 2019, *Phys. Rev. Fluids*, 4, 024603, doi: [10.1103/PhysRevFluids.4.024603](https://doi.org/10.1103/PhysRevFluids.4.024603)
 Andrés, N., Galtier, S., & Sahraoui, F. 2016a, *Physical Review E*, 94, 063206
 —. 2018, *Physical Review E*, 97, 013204
 Andrés, N., Gonzalez, C., Martin, L., Dmitruk, P., & Gómez, D. 2014, *Physics of Plasmas*, 21, 122305
 Andrés, N., Mininni, P. D., Dmitruk, P., & Gomez, D. O. 2016b, *Physical Review E*, 93, 063202
 Andrés, N., & Sahraoui, F. 2017, *Physical Review E*, 96, 053205
 Andrés, N., Sahraoui, F., Galtier, S., et al. 2019, *Physical Review Letters*, 123, 245101
 Andrés, N., Sahraoui, F., Galtier, S., et al. 2018, *Journal of Plasma Physics*, 84, 905840404, doi: [10.1017/S0022377818000788](https://doi.org/10.1017/S0022377818000788)
 Bandyopadhyay, R., Goldstein, M., Maruca, B., et al. 2020, *The Astrophysical Journal Supplement Series*, 246, 48
 Banerjee, S., & Andrés, N. 2020, *Phys. Rev. E*, 101, 043212, doi: [10.1103/PhysRevE.101.043212](https://doi.org/10.1103/PhysRevE.101.043212)
 Banerjee, S., & Galtier, S. 2013, *Physical Review E*, 87, 013019
 Banerjee, S., Hadid, L. Z., Sahraoui, F., & Galtier, S. 2016, *The Astrophysical Journal Letters*, 829, L27
 Banerjee, S., & Kritsuk, A. G. 2018, *Phys. Rev. E*, 97, 023107, doi: [10.1103/PhysRevE.97.023107](https://doi.org/10.1103/PhysRevE.97.023107)
 Batchelor, G. K. 1953, *The theory of homogeneous turbulence* (Cambridge Univ. Press)
 Benzi, R., Ciliberto, S., Tripiccion, R., et al. 1993, *Phys. Rev. E*, 48, R29
 Bertucci, C., Romanelli, N., Chaufray, J. Y., et al. 2013, *Geophysical Research Letters*, 40, 3809, doi: [10.1002/grl.50709](https://doi.org/10.1002/grl.50709)
 Bhattacharyya, D., Clarke, J. T., Bertaux, J.-L., Chaufray, J.-Y., & Mayyasi, M. 2015, *Geophysical Research Letters*, 42, 8678, doi: [10.1002/2015gl065804](https://doi.org/10.1002/2015gl065804)
 Brain, D. A. 2002, *Journal of Geophysical Research*, 107, doi: [10.1029/2000ja000416](https://doi.org/10.1029/2000ja000416)
 Brinca, A. 1991, *Cometary plasma processes*, 61, 211
 Bruno, R., & Carbone, V. 2005, *Living Reviews in Solar Physics*, 2, 4
 Bruno, R., d'Amicis, R., Bavassano, B., Carbone, V., & Sorriso-Valvo, L. 2007
 Chaffin, M. S., Chaufray, J.-Y., Stewart, I., et al. 2014, *Geophysical Research Letters*, 41, 314, doi: [10.1002/2013gl058578](https://doi.org/10.1002/2013gl058578)
 Chaffin, M. S., Chaufray, J. Y., Deighan, J., et al. 2015, *Geophysical Research Letters*, 42, 9001
 Chen, C. H. K. 2016, *Journal of Plasma Physics*, 82, 535820602, doi: [10.1017/S0022377816001124](https://doi.org/10.1017/S0022377816001124)
 Chen, C. H. K., Bale, S. D., Bonnell, J., et al. 2020, *The Astrophysical Journal Supplement Series*, 246, 53
 Clarke, J. T., Bertaux, J.-L., Chaufray, J.-Y., et al. 2014, *Geophysical Research Letters*, 41, 8013, doi: [10.1002/2014gl061803](https://doi.org/10.1002/2014gl061803)
 Clarke, J. T., Mayyasi, M., Bhattacharyya, D., et al. 2017, *Journal of Geophysical Research: Space Physics*, 122, 2336, doi: [10.1002/2016ja023479](https://doi.org/10.1002/2016ja023479)

- Coburn, J. T., Forman, M. A., Smith, C. W., Vasquez, B. J., & Stawarz, J. E. 2015, *Philosophical Transactions of the Royal Society A: Mathematical, Physical and Engineering Sciences*, 373, 20140150, doi: [10.1098/rsta.2014.0150](https://doi.org/10.1098/rsta.2014.0150)
- Coburn, J. T., Smith, C. W., Vasquez, B. J., Forman, M. A., & Stawarz, J. E. 2014, *ApJ*, 786, 52, doi: [10.1088/0004-637X/786/1/52](https://doi.org/10.1088/0004-637X/786/1/52)
- Connerney, J. E. P., Espley, J., Lawton, P., et al. 2015, *Space Science Reviews*, 195, 257
- Cowee, M. M., Gary, S. P., & Wei, H. Y. 2012, *Geophysical Research Letters*, 39, n/a, doi: [10.1029/2012gl051313](https://doi.org/10.1029/2012gl051313)
- Delva, M., Bertucci, C., Volwerk, M., et al. 2015, *Journal of Geophysical Research: Space Physics*, 120, 344, doi: [10.1002/2014JA020318](https://doi.org/10.1002/2014JA020318)
- Dmitruk, P., Matthaeus, W. H., Milano, L., et al. 2002, *The Astrophysical Journal*, 575, 571
- Edberg, N. J. T., Brain, D. A., Lester, M., et al. 2009, *Annales Geophysicae*, 27, 3537, doi: [10.5194/angeo-27-3537-2009](https://doi.org/10.5194/angeo-27-3537-2009)
- Edberg, N. J. T., Nilsson, H., Williams, A. O., et al. 2010, *Geophysical Research Letters*, 37, n/a, doi: [10.1029/2009gl041814](https://doi.org/10.1029/2009gl041814)
- Eparvier, F., Chamberlin, P., Woods, T., & Thiemann, E. 2015, *Space Science Reviews*, 195, 293
- Fang, X., Ma, Y., Brain, D., Dong, Y., & Lillis, R. 2015, *Journal of Geophysical Research: Space Physics*, 120, 10
- Ferrand, R., Galtier, S., Sahraoui, F., et al. 2019, arXiv e-prints, <https://arxiv.org/abs/1905.06110>
- Frisch, U. 1995, *Turbulence: The Legacy of A. N. Kolmogorov* (Cambridge University Press.)
- Gary, S. P. 1991, *Space Science Reviews*, 56, 373
- Grossmann, S., Lohse, D., & Reeh, A. 1997, *Phys. Rev. E*, 56, 5473
- Gruesbeck, J. R., Espley, J. R., Connerney, J. E. P., et al. 2018, *Journal of Geophysical Research: Space Physics*, 123, 4542, doi: [10.1029/2018JA025366](https://doi.org/10.1029/2018JA025366)
- Gurnett, D., Morgan, D., Duru, F., et al. 2010, *Icarus*, 206, 83
- Hadid, L., Sahraoui, F., & Galtier, S. 2017, *The Astrophysical Journal*, 838, 9
- Hadid, L., Sahraoui, F., Galtier, S., & Huang, S. 2018, *Phys. Rev. Lett.*, 120, 055102
- Halekas, J. S. 2017, *Journal of Geophysical Research: Planets*, 122, 901, doi: [10.1002/2017je005306](https://doi.org/10.1002/2017je005306)
- Halekas, J. S., Taylor, E., Dalton, G., et al. 2015, *Space Science Reviews*, 195, 125
- Halekas, J. S., Ruhunusiri, S., Harada, Y., et al. 2017, *Journal of Geophysical Research: Space Physics*, 122, 547, doi: [10.1002/2016ja023167](https://doi.org/10.1002/2016ja023167)
- Hellinger, P., Verdini, A., Landi, S., Franci, L., & Matteini, L. 2018, *The Astrophysical Journal Letters*, 857, L19
- Hendrix, D., & Van Hoven, G. 1996, *The Astrophysical Journal*, 467, 887
- Jakosky, B. M., Lin, R., Grebowsky, J., et al. 2015a, *Space Science Reviews*, 195, 3
- Jakosky, B. M., Grebowsky, J. M., Luhmann, J. G., et al. 2015b, *Science*, 350, aad0210
- Kolmogorov, A. N. 1941a, 32, 16
- . 1941b, 30, 299
- Leamon, R. J., Matthaeus, W. H., Smith, C. W., & Wong, H. K. 1998, *The Astrophysical Journal Letters*, 507, L181
- Liu, D., Yao, Z., Wei, Y., et al. 2020, *Earth and Planetary Physics*, 4, 1, doi: [10.26464/epp2020002](https://doi.org/10.26464/epp2020002)
- Ma, Y., Fang, X., Russell, C. T., et al. 2014, *Geophysical Research Letters*, 41, 6563, doi: [10.1002/2014gl060785](https://doi.org/10.1002/2014gl060785)
- MacBride, B. T., Smith, C. W., & Forman, M. A. 2008, *Astrophys. J.*, 679, 1644
- Marino, R., Sorriso-Valvo, L., Carbone, V., et al. 2008, *Astrophys. J. Lett.*, 677
- Marquette, M. L., Lillis, R. J., Halekas, J., et al. 2018, *Journal of Geophysical Research: Space Physics*, 123, 2493
- Matthaeus, W., Pouquet, A., Mininni, P. D., Dmitruk, P., & Breech, B. 2008, *Physical review letters*, 100, 085003
- Matthaeus, W., & Velli, M. 2011, *Space science reviews*, 160, 145
- Matthaeus, W. H., & Goldstein, M. 1982, *J. Geophys. Res.*, 87, 6011
- Matthaeus, W. H., Zank, G. P., Smith, C. W., & Oughton, S. 1999, *Phys. Rev. Lett.*, 82, 3444
- Mazelle, C., Cao, J., Belmont, G., Neubauer, F., & Coates, A. 1997, *Advances in Space Research*, 20, 267, doi: [https://doi.org/10.1016/S0273-1177\(97\)00544-9](https://doi.org/10.1016/S0273-1177(97)00544-9)
- Mazelle, C., Le Quéau, D., & Meziane, K. 2000, *Nonlinear Processes in Geophysics*, 77, 185

- Mazelle, C., Meziane, K., LeQueau, D., et al. 2003, *Planetary and Space Science*, 51, 785
- Mazelle, C., & Neubauer, F. M. 1993, *Geophysical research letters*, 20, 153
- Mazelle, C., Winterhalter, D., Sauer, K., et al. 2004, in *Mars' Magnetism and Its Interaction with the Solar Wind* (Springer), 115–181
- Mazelle, C. X., Meziane, K., Mitchell, D. L., et al. 2018, *Geophysical Research Letters*, 45, 3768, doi: [10.1002/2018GL077298](https://doi.org/10.1002/2018GL077298)
- Modolo, R., Chanteur, G. M., & Dubinin, E. 2012, *Geophysical Research Letters*, 39, n/a, doi: [10.1029/2011gl049895](https://doi.org/10.1029/2011gl049895)
- Osman, K. T., Matthaeus, W. H., Kiyani, K. H., Hnat, B., & Chapman, S. C. 2013, *Phys. Rev. Lett.*, 111, 201101, doi: [10.1103/PhysRevLett.111.201101](https://doi.org/10.1103/PhysRevLett.111.201101)
- Politano, H., & Pouquet, A. 1998a, *Geophysical Research Letters*, 25, 273
- . 1998b, *Physical Review E*, 57, R21
- Rahmati, A., Larson, D. E., Cravens, T. E., et al. 2017, *Journal of Geophysical Research: Space Physics*, 122, 3689, doi: [10.1002/2016ja023371](https://doi.org/10.1002/2016ja023371)
- Roberts, D., Goldstein, M., & Klein, L. 1990, *Journal of Geophysical Research: Space Physics*, 95, 4203
- Romanelli, N., Bertucci, C., Gomez, D., Mazelle, C., & Delva, M. 2013, *Planetary and Space Science*, 76, 1
- Romanelli, N., Mazelle, C., & Meziane, K. 2018, *Journal of Geophysical Research: Space Physics*, 123, 1100
- Romanelli, N., Mazelle, C., Chaufray, J.-Y., et al. 2016, *Journal of Geophysical Research: Space Physics*, 121, 11
- Romanelli, N., Modolo, R., Leblanc, F., et al. 2018a, *Geophysical Research Letters*, 45, 7891, doi: [10.1029/2018gl077714](https://doi.org/10.1029/2018gl077714)
- . 2018b, *Journal of Geophysical Research: Space Physics*, 123, 5315
- Romanelli, N., DiBraccio, G., Modolo, R., et al. 2019, *Geophysical Research Letters*, 46, 10977, doi: [10.1029/2019gl084151](https://doi.org/10.1029/2019gl084151)
- Ruhunusiri, S., Halekas, J. S., Connerney, J. E. P., et al. 2015, *Geophysical Research Letters*, 42, 8917, doi: [10.1002/2015gl064968](https://doi.org/10.1002/2015gl064968)
- . 2016, *Journal of Geophysical Research: Space Physics*, 121, 2374, doi: [10.1002/2015ja022306](https://doi.org/10.1002/2015ja022306)
- Ruhunusiri, S., Halekas, J., Espley, J., et al. 2017, *Journal of Geophysical Research: Space Physics*, 122, 656
- Russell, C., Luhmann, J., Schwingenschuh, K., Riedler, W., & Yeroshenko, Y. 1990, *Geophysical Research Letters*, 17, 897
- Sahraoui, F., Goldstein, M., Robert, P., & Khotyaintsev, Y. V. 2009, *Physical review letters*, 102, 231102
- Sahraoui, F., Hadid, L., & Huang, S. 2020, *Reviews of Modern Plasma Physics*, 4, 1
- Sorriso-Valvo, L., Marino, R., Carbone, V., et al. 2007, *Physical review letters*, 99, 115001
- Weygand, J. M., Matthaeus, W. H., Dasso, S., Kivelson, M. G., & Walker, R. J. 2007, *J. Geophys. Res.: Space Phys.*, 112, A10
- Wu, C., & Hartle, R. 1974, *Journal of Geophysical Research*, 79, 283
- Wu, C. S., & Davidson, R. C. 1972, *Journal of Geophysical Research*, 77, 5399, doi: [10.1029/ja077i028p05399](https://doi.org/10.1029/ja077i028p05399)
- Yamauchi, M., Hara, T., Lundin, R., et al. 2015, *Planetary and Space Science*, 119, 54, doi: [10.1016/j.pss.2015.09.013](https://doi.org/10.1016/j.pss.2015.09.013)

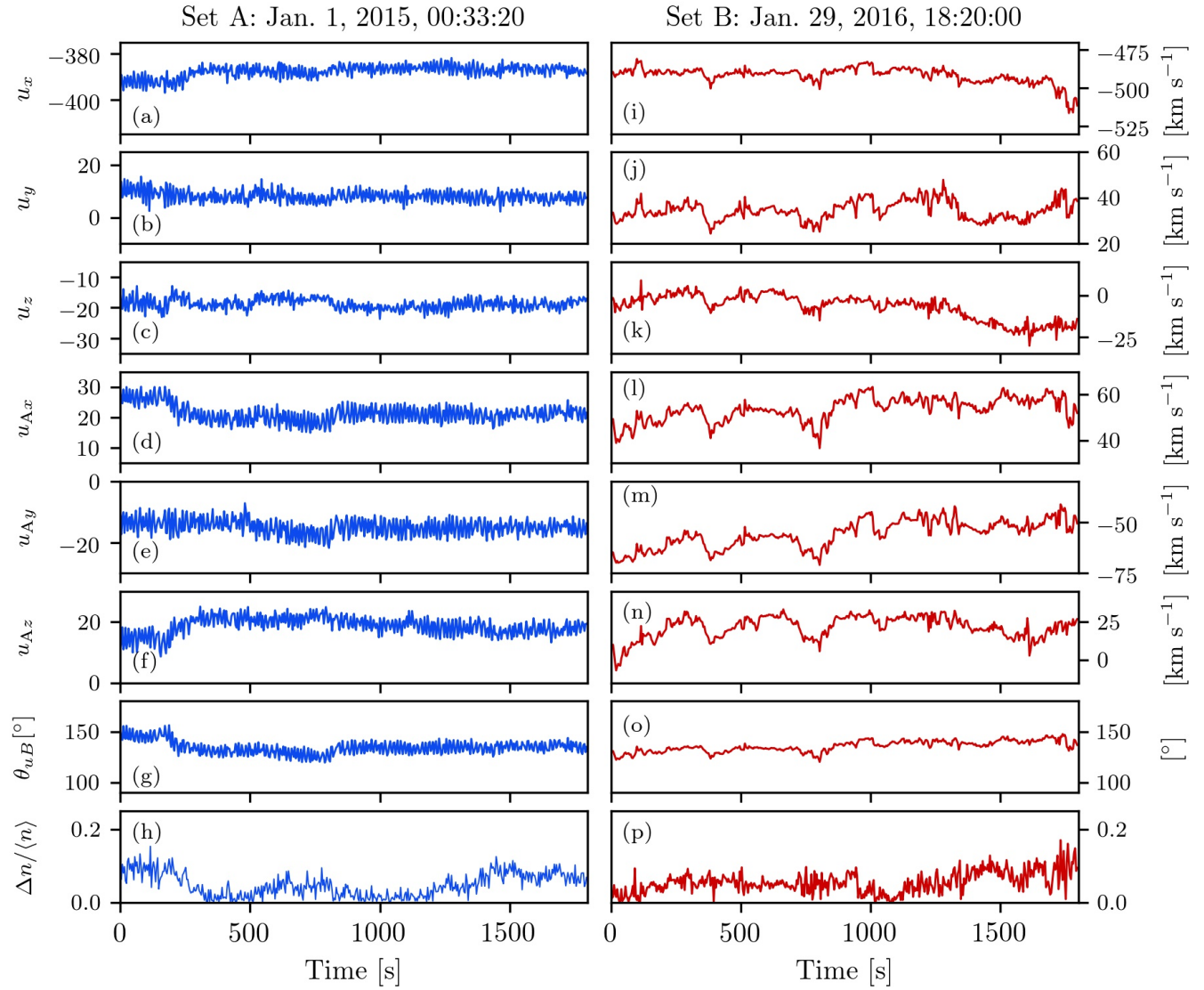


Figure 1. Time series for two examples from sets A and B. In particular, the proton and Alfvén velocity field components (in MSO coordinate system), the angle between magnetic and velocity fields and the density fluctuation level, respectively.

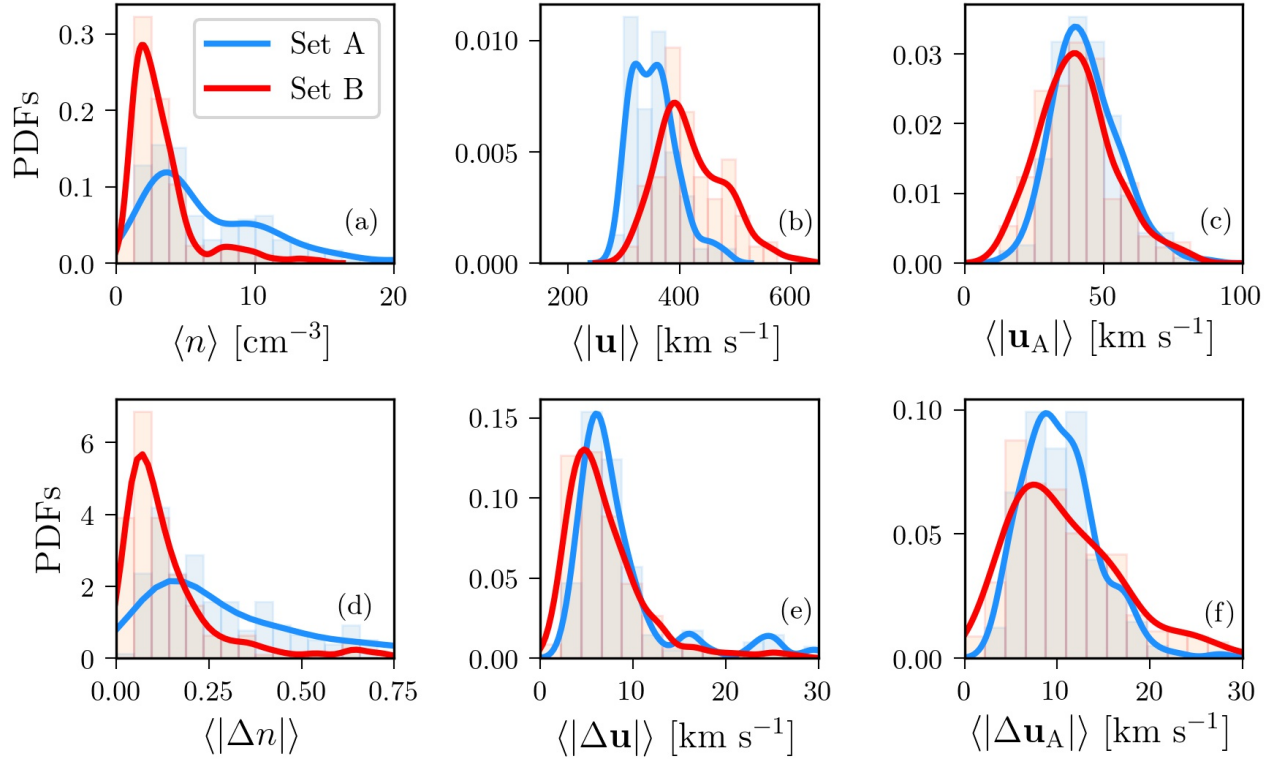


Figure 2. Probability distribution functions for (a)-(c) the number density, velocity and Alfvén velocity fields absolute values, respectively. Panels (d)-(f) show the PDFs for the fluctuation values.

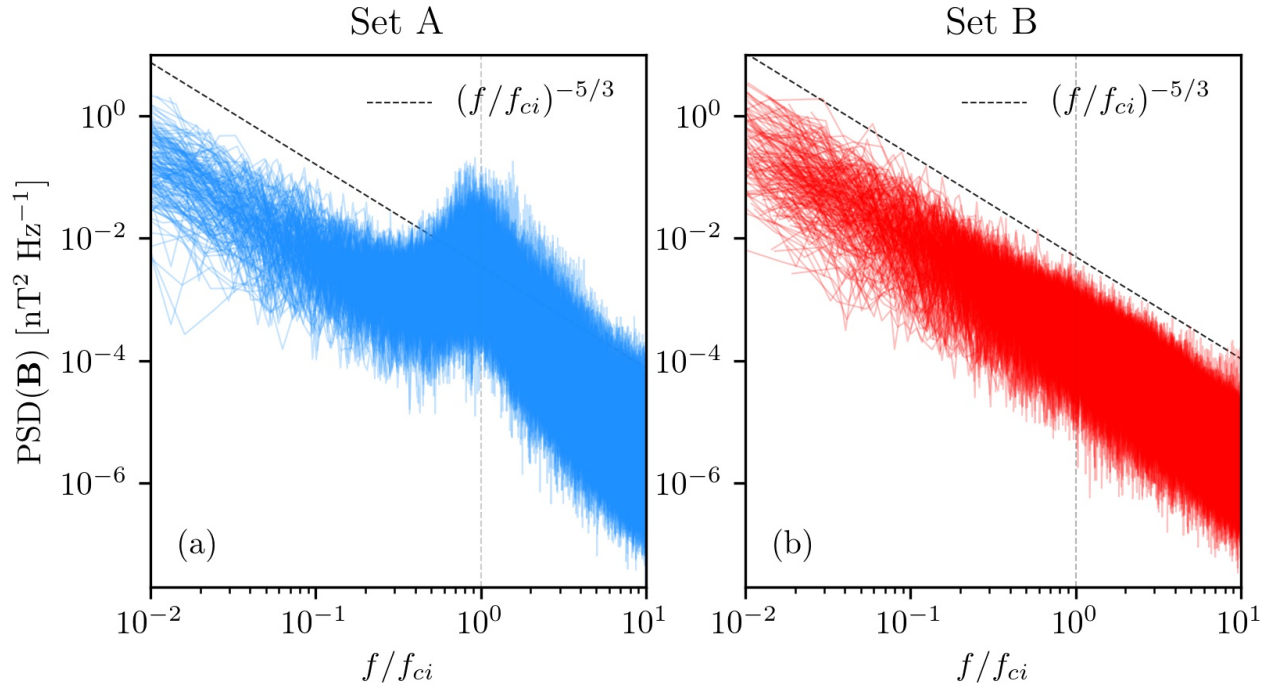


Figure 3. Magnetic power spectra density for both sets A and B, respectively.

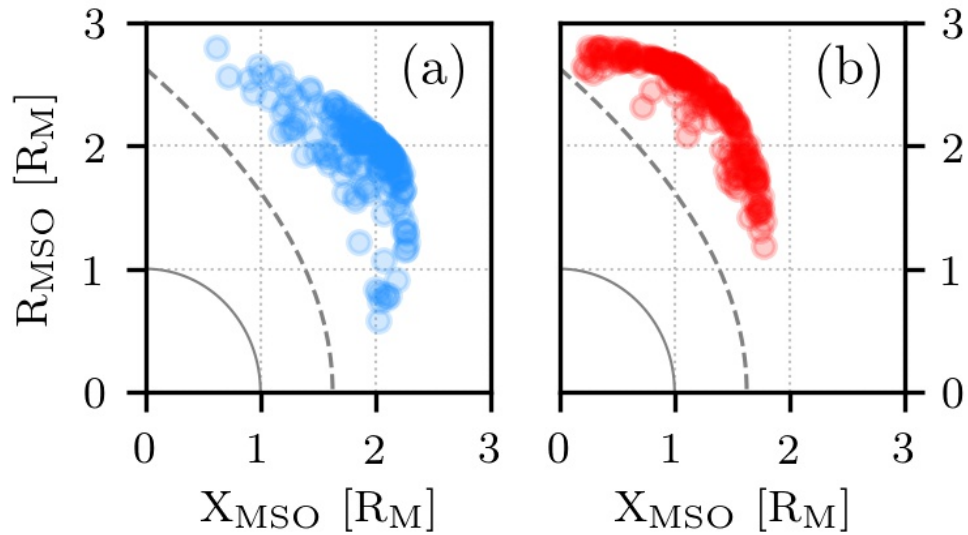


Figure 4. MAVEN location of each event in MSO reference frame for both sets. The dash gray line is the bow shock best fit from [Gruesbeck et al. \(2018\)](#).

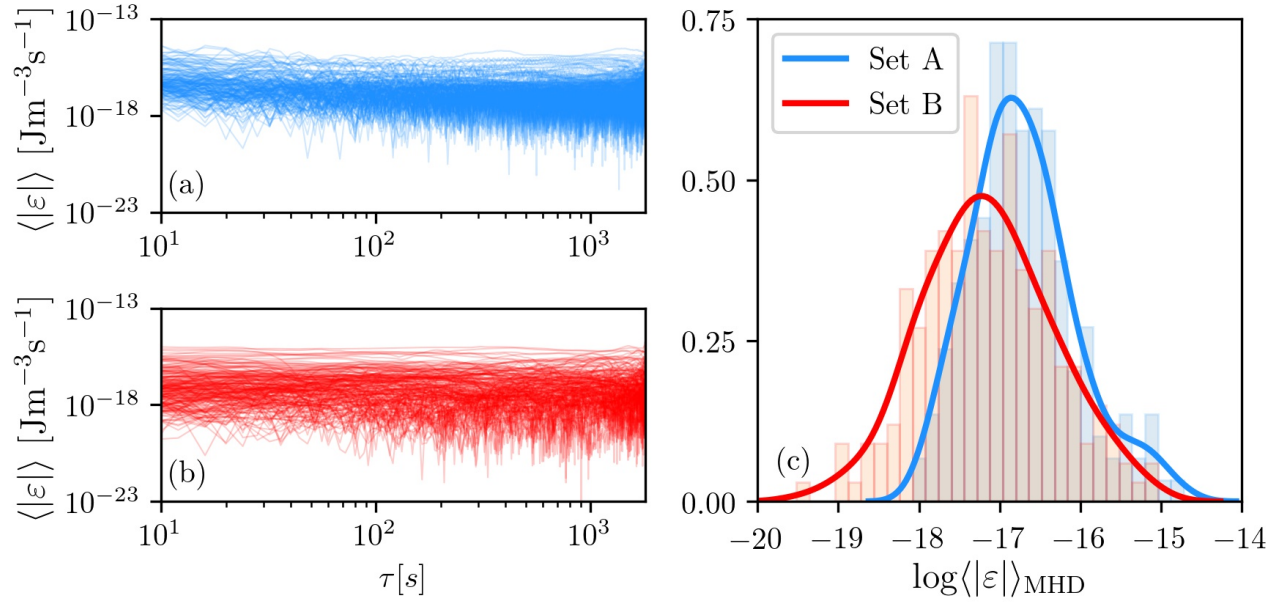


Figure 5. Energy cascade rate (absolute value) as a function of the time lag for sets (a) A and (b) B, respectively. (c) Histogram of $\log \langle |\varepsilon| \rangle_{\text{MHD}}$ for both sets.

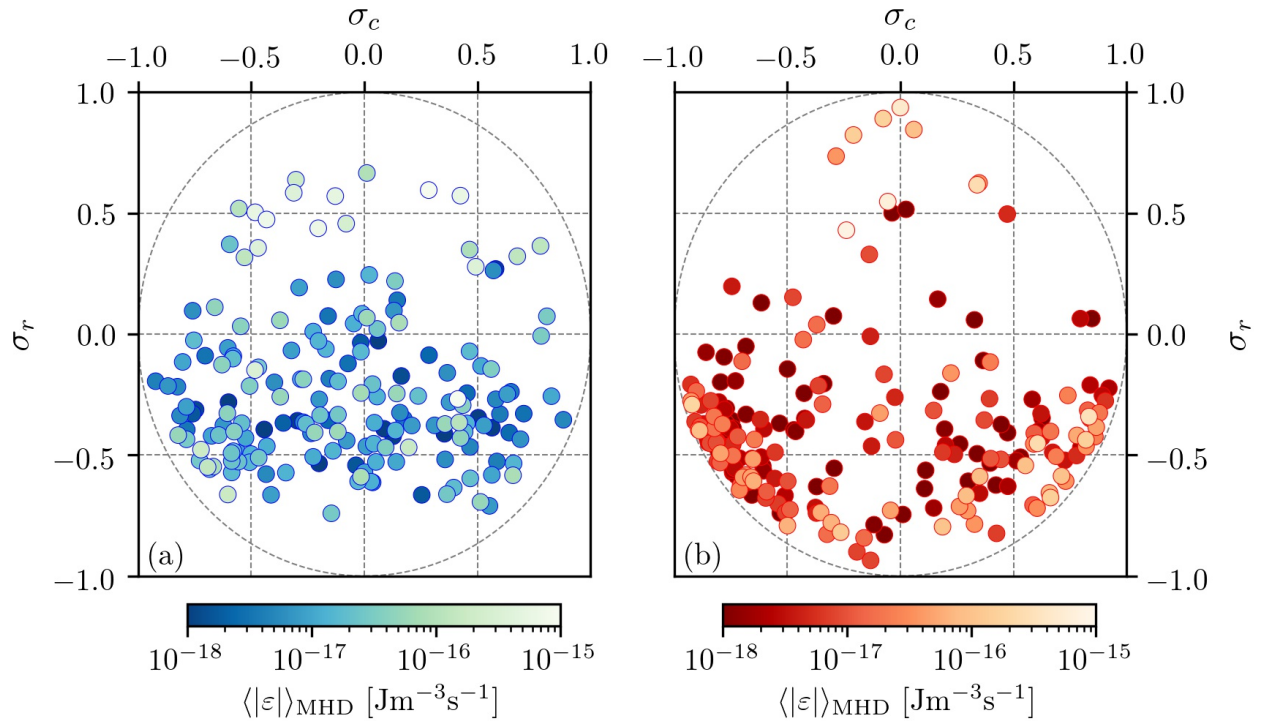


Figure 6. Scatter plot of σ_τ as a function of σ_c for both sets A and B, respectively. Color bars correspond to the mean cascade rate in the MHD scales.